Chinese Chemical Letters 36 (2025) 110147

Contents lists available at ScienceDirect

Chinese Chemical Letters

journal homepage: www.elsevier.com/locate/cclet

Near-infrared fluorescent probe with large Stokes shift and long emission wavelength for rapid diagnosis of lung cancer *via* aerosol inhalation delivery

Wenping Dong[a], Mo Ma[a,b], Jingkang Li[a], Lanlan Xu[a], Dejiang Gao[a], Pinyi Ma[a,*], Daqian Song[a,*]

[a] College of Chemistry, Jilin Province Research Center for Engineering and Technology of Spectral Analytical Instruments, Jilin University, Changchun 130012, China
[b] School of Pharmacy, Jilin University, Changchun 130012, China

ARTICLE INFO

Article history:
Received 23 April 2024
Revised 19 June 2024
Accepted 20 June 2024
Available online 21 June 2024

Keywords:
Near-infrared
Fluorescent probe
Large Stokes shift
In situ lung cancer
Rapid diagnosis

ABSTRACT

The aggressive nature and high mortality rate of lung cancer underscore the imperative need for early diagnosis of the disease. Thus, aminopeptidase N (APN), a potential biomarker for lung cancer, should be thoroughly investigated in this context. This report describes the development of **HA-apn**, a novel near-infrared fluorescent probe, specifically engineered for the sensitive detection of endogenous APN. Characterized by its high selectivity, straightforward molecular architecture, and suitable optical properties, including a long-wavelength emission at 835 nm and a large Stokes shift of 285 nm, **HA-apn** had high efficacy in identifying overexpressed APN in tumor cells, which shows its potential in pinpointing malignancies. To further validate its applicability and effectiveness in facilitating the direct and enhanced visualization of pulmonary alterations, an *in situ* lung cancer mouse model was employed. Notably, **HA-apn** was applied for *in vivo* imaging of APN activity in the lung cancer mouse model receiving the probe through aerosol inhalation, and rapid and precise diagnostic results were achieved within 30 min post-administration. Overall, **HA-apn** can be applied as an effective, non-intrusive tool for the rapid and accurate detection of pulmonary conditions.

Lung cancer is a leading adversary that has challenged public health with its high incidence and mortality rates. Annually, it accounts for approximately 2 million new cases and 1.76 million deaths worldwide [1,2]. This makes it not only the most commonly diagnosed cancer but also the foremost cause of cancer-related mortality [3-5]. The pivotal role of early diagnosis in curtailing lung cancer mortality has been well-recognized [6]. It also highlights an urgent need for advancements of the current diagnostic methodologies. The current clinical practices for lung cancer detection primarily rely on surgical biopsies and computed tomography (CT) imaging, which have limitations [7]. These methods are invasive and often subject patients to harmful ionizing radiation, thereby posing additional health risks [8-10]. Moreover, the reliance on empirical judgment by clinicians further underscores the necessity for more objective and less invasive diagnostic alternatives.

Recent research has illustrated the potential of exploiting disease biomarkers for non-invasive diagnostic approaches [11-13]. For example, certain studies have successfully employed specific enzymes to achieve fluorescent imaging of lung cancer, offering new avenues for the early diagnosis and treatment of the disease [14-19]. In this context, aminopeptidase N (APN), also known as CD13 or alanine aminopeptidase, has emerged as a particularly important enzyme. As a membrane-bound zinc exopeptidase, APN plays a crucial role in a wide array of physiological and pathological processes [20-22]. Aberrant expression and catalytic functions of APN are linked to the pathogenesis of several diseases, including bladder cancer [23], hepatocellular carcinoma [24-27], breast cancer [28,29], cervical cancer [30] and renal carcinoma [31], wherein the overexpression of APN has been observed. For this reason, APN is a promising tumor biomarker. Despite the importance of APN in various cancers, its recognition as a biomarker for lung cancer remains largely underexplored.

To address this unmet need, our research presents the synthesis of a novel fluorescent probe **HA-apn**. This involved covalently attaching *p*-aminobenzyl alcohol to fluorophore **HA** and in-

* Corresponding authors.
E-mail addresses: mapinyi@jlu.edu.cn (P. Ma), songdq@jlu.edu.cn (D. Song).

https://doi.org/10.1016/j.cclet.2024.110147
1001-8417/

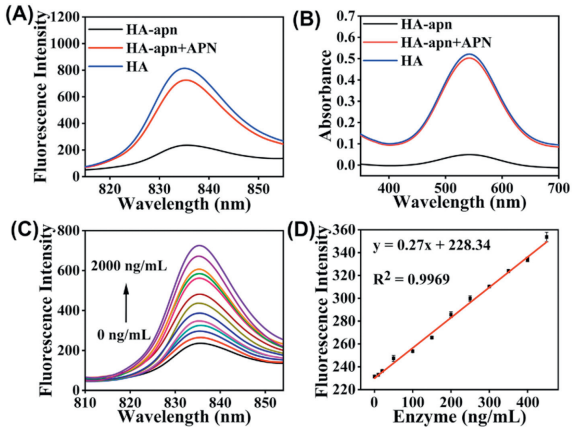

Fig. 1. (A) Fluorescence and (B) absorption spectra of 10 μmol/L **HA-apn** and reaction system (10 μmol/L **HA-apn** and 2000 ng/mL APN). (C) Fluorescence spectra of 10 μmol/L **HA-apn** in the presence of APN at various concentrations. (D) Linear relationship between fluorescence intensity at 835 nm of reaction system and APN concentration (0–450 ng/mL).

corporating L-alanine residues. This near-infrared (NIR) fluorescent probe had a large Stokes shift of 285 nm and was specifically and strategically designed for the sensitive detection of APN. Upon interacting with APN, the probe undergoes a reaction triggered by the recognition and hydrolysis of the alanyl group, leading to the release of the **HA** fluorescent group and a pronounced change in fluorescence intensity. **HA-apn** was characterized by its exceptional tissue penetration depth and enhanced signal-to-noise ratio in physiological conditions. These features were validated using an *in situ* murine model of lung cancer. By administering **HA-apn** through aerosol inhalation, the rapid, clear visualization of APN activity in the lung tissues of the mouse model was achieved within only 30 min. With its high efficiency and non-invasiveness, **HA-apn** can potentially be employed as a powerful diagnostic tool for the swift and precise identification of lung-associated diseases. Scheme S1 (Supporting information) illustrates the synthetic pathway of **HA-apn**.

The spectral characteristics of **HA-apn** are pivotal to the evaluation of APN detection capability. Initial investigations into the fluorescence and absorption spectra revealed that the emission peak of **HA-apn** at 835 nm was notably enhanced following the addition of APN, which closely aligns with the emission characteristics observed for **HA** (Fig. 1A). Similarly, absorption spectroscopy showed a significant increase in the absorption peak of **HA-apn** at 550 nm upon APN addition, which corresponds to the absorption profile of **HA** (Fig. 1B). These findings indicate the potential of **HA-apn** in fluorescence-based and colorimetric APN detection techniques.

Further investigations into the properties of **HA-apn** delineated its response dynamics, stability across a range of pH values, photostability, and thermal behavior. The fluorescence intensity of **HA-apn** gradually increased during the first 120 min, after which it reached a plateau and remained stable (Fig. S7 in Supporting information). The fluorescence intensity of **HA-apn** was unaffected across a range of pH values, and the optimal enzymatic activity of APN was observed at a neutral pH of 7.4 (under acidic and alkaline conditions, the activity of APN is poor or even inactivated, so the response effect between probe **HA-apn** and APN is poor), as presented in Fig. S8 (Supporting information). Photostability experiments, conducted under light at 550 nm, verified the resistance of **HA-apn** to photodegradation over a period of 105 min (Fig. S9 in Supporting information). Assessments of thermal stability indicated that **HA-apn** was able to maintain its fluorescence intensity within the temperature range of 25–42 °C. Importantly, the fluorescence intensity of the reaction system increased with increasing

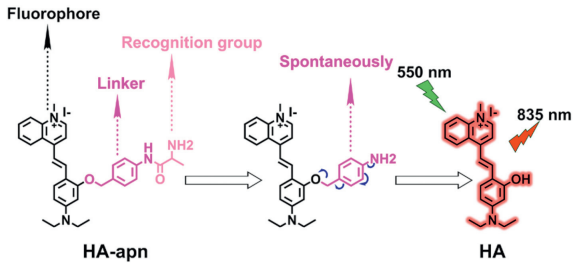

Fig. 2. The proposed APN-detection mechanism of **HA-apn**.

temperature, reaching its optimal level at 37 °C. This suggests that the rate of enzymatic reactions is accelerated within this temperature range (Fig. S10 in Supporting information). Based on these observations, all subsequent experiments were carried out in phosphate buffered saline (PBS, 10 mmol/L, pH 7.4) at a physiological temperature of 37 °C for 120 min.

The analytical performance of **HA-apn** was evaluated using the fluorescence method under the optimal conditions. Analysis of the fluorescence spectra, as illustrated in Figs. 1C and D, revealed the progressive increase in fluorescence intensity at 835 nm with rising APN concentrations ($\lambda_{ex} = 550$ nm). This observation is further substantiated by the robust linear correlation ($R^2 = 0.9969$) between the fluorescence intensity and APN concentration in the 0–450 ng/mL range and the low detection limit of 0.63 ng/mL. Further, the kinetics of the enzymatic reaction between **HA-apn** and APN were studied. Derived from the Michaelis-Menten and Lineweaver-Burk plots presented in Figs. S11 and S12 (Supporting information), respectively, the Michaelis constant (Km) was 2.20 μmol/L. Comparative analysis summarized in Table S1 (Supporting information) showed the superiority of **HA-apn** over other reported fluorescent probes, according to its superior performance metrics such as excitation/emission wavelengths, detection limit, and Stokes shift. Consequently, **HA-apn** is a highly potential tool in fluorescence spectroscopy for quantitative detection of APN.

The selectivity of **HA-apn** is crucial for the accurate detection of analytes within complex biological matrices. To assess the specificity of **HA-apn** toward APN, the influence of various potential interferences such as different cations, anions, amino acids, and enzymes was investigated. The results presented in Fig. S13 (Supporting information) demonstrated that **HA-apn** was able to maintain its high performance despite the presence of interfering substances at high concentrations. In contrast, the introduction of APN significantly impacted **HA-apn**, and this impact can be attributed to alanine, the APN-specific recognition element in the probe. Consequently, **HA-apn** shows considerable potential in the selective detection of APN in complex biological systems, including the potential in precision diagnostics.

The sensing response mechanism of **HA-apn** towards APN was studied using mass spectrometry and high performance liquid chromatography (HPLC) analysis. The mass spectrometric results showed a mass peak of the reaction system at *m/z* 333.1907 (Fig. S14 in Supporting information), which was consistent with the mass peak of **HA** (*m/z* 333.1964) (Fig. S3 in Supporting information). The HPLC analysis (Fig. S15 in Supporting information) showed the characteristic peak of **HA-apn** at 2.85 min and **HA** at 3.35 min. The reaction system also exhibited the characteristic peaks at 2.89 and 3.38 min, which coincided with the peaks of **HA-apn** and **HA**, respectively. Based on the results presented above, it is possible that the sensing mechanism of APN by **HA-apn** (Fig. 2) involves the specific recognition and cleavage of the alanine residue on **HA-apn**. This then leads to the spontaneous departure of the p-aminophenol linker, resulting in the release of **HA**, which enables the detection of APN.

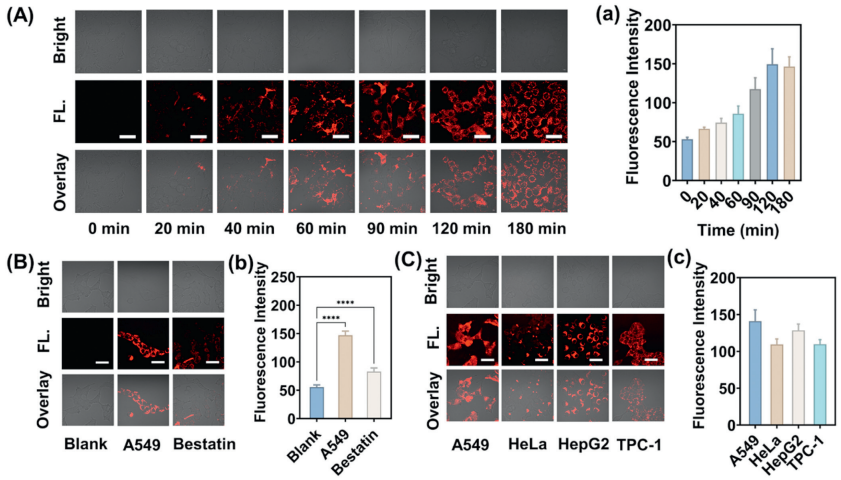

Fig. 3. (A) Variation of intracellular fluorescence intensity over time. (a) Mean fluorescence intensity of cells in (A). (B) Variation of intracellular fluorescence intensity with and without inhibitors. (b) Mean fluorescence intensity of cells in (B). (C) Fluorescence images of different cell lines incubated with APN. (c) Mean fluorescence intensity of cells in (C). Scale bar: 20 μm. Data are presented as mean ± standard deviation (SD) ($n = 5$); $^{****}P < 0.0001$.

To understand the spectral changes of the fluorescent probe before and after the reaction with APN, theoretical calculations were performed on the molecules, and the results are shown in Fig. S16A (Supporting information). Comparing the electron-hole orbit diagrams for **HA-apn** before and after the reaction with **HA** revealed that **HA** exhibited a more pronounced intramolecular charge transfer effect compared to **HA-apn**. For this reason, it led to more significant changes in fluorescence. Molecular docking experiments were conducted to investigate the binding of **HA-apn** to APN, and the findings are illustrated in Fig. S16B (Supporting information). The molecule was found to fit into the active site of APN. The recognition group was observed to form a strong hydrogen bond with the amino acid ASN947 and exhibit weak interactions with six other surrounding amino acids. The binding energy was calculated to be −9.1 kcal/mol, an indication of a strong interaction between **HA-apn** and APN, which can help facilitate the sensing mechanism of the probe.

To evaluate the suitability of **HA-apn** as an imaging agent of APN in cells, we first assessed its cytotoxicity in A549, HeLa, TPC-1 and HepG2 cells using the cell counting kit-8 (CCK-8) assay. As illustrated in Fig. S17 (Supporting information), **HA-apn** exhibited low cytotoxicity with a cell survival rate exceeding 90% even at a high concentration of 100 μmol/L. Further, the biocompatibility of **HA-apn** was confirmed through a hemolysis assay. The results showed that the hemolysis rate was lower than 5% after 3 h of incubation with **HA-apn** at a concentration of up to 50 μmol/L (Fig. S18 in Supporting information). This finding indicates the suitability of **HA-apn** for cell imaging.

To elucidate the dynamics of the cellular uptake of **HA-apn**, we quantitatively analyzed the evolution of intracellular fluorescence intensity as a function of time. As depicted in Fig. 3A, the augmentation in fluorescence intensity within the cellular milieu was discernible over the observed period. Notably, the cellular uptake of **HA-apn** was manifested as a pronounced surge in fluorescence within the initial 2-h timeframe before reaching a plateau, where saturation in the intracellular accumulation of **HA-apn** was reached. Given this temporal profile, it is evident that a 2-h period is the optimal incubation time; thus, it was employed in subsequent **HA-apn**-mediated cell imaging experiments.

The fluorescence signal produced by A549 cells was suppressed upon the addition of the inhibitor bestatin, confirming that the observed signal was a result of **HA-apn**'s response to endogenous APN (Fig. 3B). Additionally, the enzymatic activity of APN was assessed using the probe **HA-apn** across a range of cancer cell lines, including A549 (lung carcinoma), HeLa (cervical cancer), TPC-1 (thyroid cancer), and HepG2 (hepatocellular carcinoma). Differential APN activity, as evidenced by **HA-apn**-mediated fluorescence, was observed among these cell types (Fig. 3C). These findings not only confirm the high specificity of **HA-apn** towards APN as a fluorescent probe but also highlight its potential as a diagnostic tool for evaluating APN activity *in situ*. The observed differences in APN activity across the tested cell lines further suggest the feasibility of utilizing **HA-apn** in a variety of cancer types, which can broaden its application in cancer diagnostics and research.

After the successful *in vitro* validation, we proceeded to assess the *in vivo* imaging efficacy of the HA-apn probe by intravenously inoculating mice with A549 cells *via* the tail vein to establish an *in situ* lung cancer model [32,33]. The successful establishment of the *in situ* lung cancer mouse model was confirmed through H&E staining analysis of both normal and tumorous lung tissues (Fig. S19 in Supporting information). The animal experiment was carried out under the ethical protocols set by Jilin University's Institutional Animal Care and Use Committee (IACUC), certified by the ethical inspection permit number SY202306031.

The APN expression varied across different cancer types, as evidenced by experiments conducted in various cell lines. The conventional imaging approach through tail-vein administration can compromise the probe targeting. **HA-apn** (500 μmol/L, 200 μL) was administered intravenously into an *in situ* lung cancer mouse model. In subsequent fluorescence imaging conducted 30 min post-injection, fluorescence signals were not detected in the lungs, despite the successful establishment of the *in situ* lung cancer model (Fig. S20 in Supporting information). This appears to be due to the lack of targeting in the lung, which can be attributed to two main factors: (1) the challenges associated with the competitive distribution of the probe *via* the bloodstream to the lungs and other organs; (2) the consumption of the probe by APN present in other organs and in circulating blood can interfere with the lung-targeting ability of the probe during imaging [34-37].

To address the targeting issue, we adopted an aerosol inhalation administration approach. This method enables aerosolized probes to be deposited directly in the lungs, thereby enhancing the targeting efficiency and bioavailability in lung tumors. We conducted a time-dependent study by administering **HA-apn** to mice *via* aerosol inhalation (Fig. 4A). After placing the lung cancer mice in a specially prepared nebulization device, aerosol inhalation was

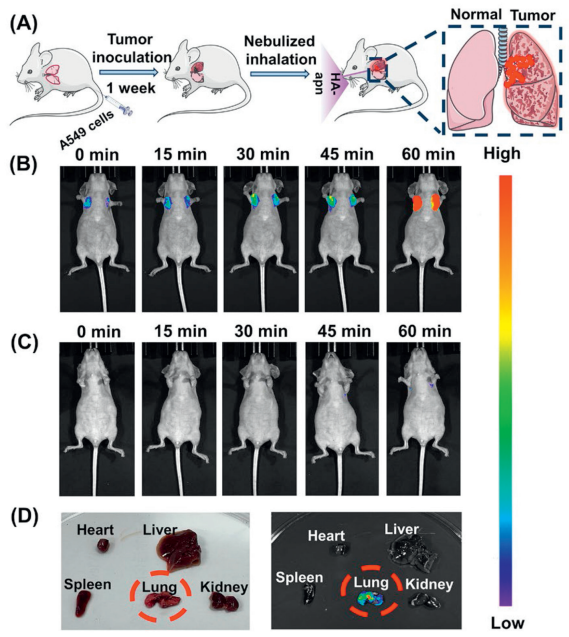

Fig. 4. (A) Experimental diagram displaying the establishment of *in situ* cell lung mouse model *via* A549 cell injection through the tail vein and the administration of probe **HA-apn** (500 μmol/L, 4 mL) *via* aerosol inhalation. (B) Time-varying images of *in situ* lung cancer mice after inhalation of probe **HA-apn** (500 μmol/L, 4 mL). (C) Time-varying images of healthy mice after inhalation of probe **HA-apn** (500 μmol/L, 4 mL). (D) Fluorescence images of the heart, liver, spleen, lungs, and kidneys of mice.

commenced for 30 min before fluorescence imaging. Remarkably, distinct fluorescence signals were observed in the lungs of mice within only 30 min post-aerosol inhalation. The fluorescence intensity in the lungs increased over time and reached its peak at 60 min (Fig. 4B). This experiment was also replicated in healthy mice, and no fluorescent signals were observed in the lungs of these mice after 30 min of aerosol inhalation administration; the increase in fluorescence intensity was also not observed over time (Fig. 4C). The corresponding fluorescence intensities are shown in Fig. S21 (Supporting information). These results indicate that the expression of APN in the lungs of mice with lung cancer is elevated, which can allow for the rapid diagnosis of lung cancer through aerosol inhalation of **HA-apn** probe.

After the imaging studies, we proceeded to dissect the mice and harvest their major organs for fluorescence imaging analysis. The examination revealed that the fluorescence emission from the lungs was markedly more intense compared to that from other organs (Fig. 4D). This observation suggests that through inhalation administration, **HA-apn** can precisely target pulmonary tumors. By leveraging its high specificity to APN, **HA-apn** has the potential for the early diagnosis of lung cancer through imaging.

In conclusion, this study proposes a novel near-infrared fluorescent probe, **HA-apn**, for the evaluation of APN expression level in lung cancer and its potential as a biomarker for the disease. The probe **HA-apn** had high stability, good solubility, long emission wavelength (835 nm), and large Stokes shift (285 nm), this is suitable for the accurate and sensitive detection of APN through fluorometric and colorimetric methods. In bioimaging, we created an *in situ* mouse model of lung cancer to provide a clearer and more direct observation of the lung environment. In addition, we used an aerosol inhalation delivery method, which was found to be more suited to the imaging and confirmation of APN overexpression in lung cancer cells. Surprisingly, strong fluorescent signals were observed in the lungs of the lung cancer mouse model after 30 min of aerosol inhalation, and the imaging results showed that the targeting ability of **HA-apn** was improved. The imaging outcomes suggest that **HA-apn** holds considerable promise as an expedient tool for the rapid diagnosis of lung cancer.

Declaration of competing interest

The authors declare that they have no known competing financial interests or personal relationships that could have appeared to influence the work reported in this paper.

CRediT authorship contribution statement

Wenping Dong: Writing – original draft, Validation, Investigation, Data curation, Conceptualization. **Mo Ma:** Investigation, Data curation. **Jingkang Li:** Investigation, Data curation. **Lanlan Xu:** Investigation, Data curation. **Dejiang Gao:** Software, Formal analysis. **Daqian Song:** Supervision, Resources, Project administration, Funding acquisition.

Acknowledgments

This work was supported by the National Natural Science Foundation of China (Nos. 22004046 and 22074052) and the Science and Technology Developing Foundation of Jilin Province of China (Nos. 20240404044ZP, 20230101033JC and 20220505015ZP).

Supplementary materials

Supplementary material associated with this article can be found, in the online version, at doi:10.1016/j.cclet.2024.110147.

References

[1] A.A. Thai, B.J. Solomon, L.V. Sequist, et al., Lancet 398 (2021) 535–554.
[2] H.M. Abdelaziz, M. Gaber, M.M. Abd-Elwakil, et al., J. Control. Release 269 (2018) 374–392.
[3] F. Bray, M. Laversanne, E. Weiderpass, I. Soerjomataram, Cancer 127 (2021) 3029–3030.
[4] S. Geiger, D. Hirsch, F.G. Hermann, Eur. Respir. Rev. 26 (2017) 170044.
[5] Y. Li, B. Yan, S. He, Biomed. Pharmacother. 169 (2023) 115891.
[6] D. Marzorati, L. Mainardi, G. Sedda, et al., J. Breath Res. 13 (2019) 034001.
[7] X. Song, R. Wang, J. Gao, et al., Chin. Chem. Lett. 33 (2022) 1567–1571.
[8] G. Giaccone, Y. He, Semin. Cancer Biol. 94 (2023) 1–10.
[9] L. Osmani, F. Askin, E. Gabrielson, Q.K. Li, Semin. Cancer Biol. 52 (2018) 103–109.
[10] X. Yua, H. Ma, G. Xu, Z. Liu, Chin. Chem. Lett. 33 (2022) 4169–4174.
[11] X. Li, D. Shi, Y. Song, et al., Chin. Chem. Lett. 33 (2022) 1572–1576.
[12] Y. Sun, X. Zhou, L. Sun, et al., Chin. Chem. Lett. 33 (2022) 4229–4232.
[13] H. Pan, X. Chai, J. Zhang, Chin. Chem. Lett. 34 (2023) 108321.
[14] E.M. Digby, O. Sadovski, A.A. Beharry, Chemistry 26 (2020) 2713–2718.
[15] S. Son, M. Won, O. Green, et al., Angew. Chem. Int. Ed. 58 (2019) 1739–1743.
[16] J. Yan, K. Wang, L. Gui, et al., Anal. Chem. 95 (2023) 14402–14412.
[17] X. Zhang, C. Jiang, T. He, et al., Anal. Chem. 94 (2022) 3227–3234.
[18] X. Zhang, K. Jiang, S. Jiang, et al., Anal. Chem. 94 (2022) 13770–13776.
[19] X. Zhang, X. Li, W. Shi, H. Ma, Chem. Commun. 57 (2021) 8174–8177.
[20] A.T. Look, R.A. Ashmun, L.H. Shapiro, S.C. Peiper, J. Clin. Invest. 83 (1989) 1299–1307.
[21] Y. Aozuka, K. Koizumi, Y. Saitoh, et al., Cancer Lett. 216 (2004) 35–42.
[22] L. Feng, Z. Tian, M. Zhang, et al., Chin. Chem. Lett. 32 (2021) 3053–3056.
[23] J. Huang, Y. Jiang, J. Li, et al., Angew. Chem. Int. Ed. 59 (2020) 4415–4420.
[24] X. He, Y. Hu, W. Shi, et al., Chem. Commun. 53 (2017) 9438–9441.
[25] X. He, Y. Xu, W. Shi, H. Ma, Anal. Chem. 89 (2017) 3217–3221.
[26] H. Li, Y. Li, Q. Yao, et al., Chem. Sci. 10 (2019) 1619–1625.
[27] M. Ma, D. Dai, P. Ma, et al., Sens. Actuators B: Chem. 379 (2023) 133228.
[28] H. Li, Q. Yao, W. Sun, et al., J. Am. Chem. Soc. 142 (2020) 6381–6389.
[29] Y. Liu, C. Xu, H. Liu, et al., Anal. Chem. 93 (2021) 6463–6471.
[30] J. Yang, C. Shen, T. Zhu, et al., Biomater. Sci. 11 (2023) 2809–2817.
[31] D. Lu, B. Yuan, Q. Ye, et al., Sens. Actuators B: Chem. 395 (2023) 134494.
[32] Y. Xu, M. Cui, W. Zhang, et al., Chem. Eng. J. 428 (2022) 132514.
[33] W.L. Qiu, W.H. Hsu, S.M. Tsao, et al., Polymers 13 (2021) 4353.
[34] C. Oh, O.H. Jeon, J. Han, et al., ACS Appl. Nano Mater. 6 (2023) 3693–3703.
[35] S. Mangal, W. Gao, T. Li, Q. Zhou, Acta Pharmacol. Sin. 38 (2017) 782–797.
[36] Y.H. Quan, C.H. Oh, D. Jung, et al., JAMA Surg. 155 (2020) 732.
[37] L. Wang, Y. Rao, X. Liu, et al., J. Nanobiotechnol. 19 (2021) 56.